AIAA SciTech Forum
January 3-7, 2022, San Diego, CA & Virtual
AIAA SCITECH 2022 Forum

10.2514/6.2022-0728

Computational study on gliding flight of a damselfly

Yu Pan[a, 1], Zixi Zhang[b, 2] and Haibo Dong[a, 3]
[a]*Department of Mechanical and Aerospace Engineering, University of Virginia, Charlottesville, Virginia, 22904, USA*
[b]*School of Civil and Environmental Engineering, Georgia Institute of Technology, Atlanta, Georgia, 30332, USA*

Gliding flight is commonly accepted to be a valuable energy-saving mechanism used by natural flyers. In this work, In this work, the gliding flight of a damselfly undergoing was filmed in a large flight enclosure by using three orthogonally arranged and synchronized high-speed cameras. Using a 3D subdivision surface reconstruction methodology, the damselfly's wing deformation and kinematics were modeled and reconstructed from the high-speed videos. An immersed-boundary-method-based Navier-Strokes equation solver is then employed to compute the aerodynamic performance of damselfly in gliding flight. A comparison between the aerodynamics of solitary wings and the fore-hind wing system suggests that wing-wing interactions can reduce the drag of the forewing and improve its gliding performance. Three Euler angles are employed to define the orientation of the wings in gliding. Parametric studies on these angles are implemented to obtain the optimal orientation of the wings in gliding flight. It is found that the wings with the orientation directly obtained from the experiments achieve the optimal gliding performance among all cases. In addition, vortex structures and surface pressure are also compared and analyzed to better understand the gliding aerodynamics, which can be used for the flight control of flapping-wing micro air vehicles.

I. Nomenclature

θ	=	pitching angle
ϕ	=	flapping angle
ψ	=	deviation angle
β	=	body angle
α	=	glide angle
c	=	chord length of the forewing
L	=	wing length of the forewing
C_Y	=	vertical force coefficient
C_X	=	horizontal force coefficient
r	=	the ratio of vertical force to the horizontal force
f	=	flapping frequency
o-xyz	=	wing-root coordinate system
O-XYZ	=	body-fixed coordinate system
Re	=	Reynolds number
S	=	the area of the wing
U_∞	=	the velocity of the wing in gliding

II. Introduction

In nature, the main source of lift and propulsion for insects is flapping their wings. Gliding flight is usually thought to be energy-saving for birds. Tremendous studies have shown birds can achieve efficient lift-generating through gliding

[1] Graduate student, yp8xd@virginia.edu, AIAA Student Member.
[2] Graduate student, zzhang942@gatech.edu, summer visiting student at UVA
[3] Professor, haibo.dong@virgnia.edu, AIAA Associate Fellow.

flight. The fixed-wing flight makes birds generate an elliptic lift uniformly distributed across the span and the smallest amount of induced drag. However, gliding is an uncommon mode of insect flight[1]. It has been reported that only several insects, including dragonflies, locusts and butterflies, glide frequently for different reasons[1]. One reason for frequently gliding flight is energy-saving as it requires virtually no effort from insects[2]. In gliding flight, the airflow over an insect can be considered to be steady and the insect makes use of potential energy to move horizontally above the ground. The other reason may be thermoregulatory[3]. At high temperatures, insects may run the risk of overheating during active flapping flight, gliding can enable insects to benefit from convective cooling by moving quickly through the air without extra heat production. Engineers and fluid dynamists are more attracted to reveal the underlying energy-saving mechanisms and find the optimal gliding strategies, which is important to design energy-saving micro aerial vehicles.

One of the main limitations of insect-scale flying robots is aerodynamically unfavorable scaling laws that result in increased cost of transport as the size is reduced. Inspired from nature, a hybrid flapping-gliding flight mode is thought to be a promising locomotion strategy to minimize the energetic cost of locomotion[4]. However, gliding flight, especially on insects, received little attention. The forces on gliding dragonfly wings have previously been measured from rectangular planform wings[5] or real dragonfly wings attached to a metal shaft[6]. These studies are different from real free gliding and did not include the variation of wing orientation. Recently, the free gliding flight of the damselfly Hetaerina Americana was filmed in a large flight enclosure by using a high-resolution photogrammetry system [7]. In their work, the damselfly's wing deformation and kinematics were modeled and reconstructed from the high-speed videos using a 3D subdivision surface reconstruction methodology. Based on the work, the orientation of wings in gliding flight has been obtained and a parametric study is carried out to find the optimal wing orientation of the damselfly in gliding flight.

In this paper, the original wing orientation of damselfly in gliding flight is extracted as the baseline case. An immersed-boundary-method-based Navier-Strokes equation solver is employed to compute the aerodynamic performance damselfly in gliding flight. A comparison between the aerodynamic performance of solitary wings and fore-hind wing system reveals the role of wing-wing interaction in the gliding flight of a damselfly. Besides, three Euler angles are defined in a wing-root coordinate frame to describe the wing orientation in gliding flight: the flapping angle ϕ, the deviation angle ψ, and the pitching angle θ. Then, a parametric study on these Euler angles is implemented to obtain the optimal orientation of the wing during gliding flight. An outline of the chapters is as follows: Sec. III describes the definition of wing orientation, the numerical methods, the simulation setup, and the definition of performance parameters. The results and discussions are presented in Sec. IV. The conclusions are given in Sec. V.

III. Problem Definition and Numerical Approach

A. Damselfly wing model and orientation definition

The gliding motion of damselfly has been recorded by high-speed videos. The wings' deformation and kinematics are modeled and reconstructed from the videos in Autodesk Maya (Autodesk Inc.). Figure 1(a) shows the snapshots of damselfly at two sequenced positions during the gliding flight. It can be seen that wings are at a fixed orientation to the body in gliding flight. Also, the body angle β, the angle between the body and the ground (shown in Fig. 1(b)), keeps at $8^\circ \pm 2^\circ$ which is measured from the experiments. The red arrow in Fig. 1(a) denotes the gliding direction, which denotes the damselfly glides at an angle α from the horizontal. The angle is called the glide angle[1] and is $50^\circ \pm 3^\circ$ which can be obtained by dividing the gliding velocity U_∞ into horizontal velocity u and vertical velocity v (Fig. 1(b)). This angle is much larger than that of a dragonfly[1], which shows the particularity of the damselfly in the current work. Because the glide time is very short and the variation of glide speed is small, we take the gliding flight as steady in this work. For the gliding flight, the descending motion, forward motion, and the corresponding forces should be mainly studied and analyzed. Thus, a body-fixed frame O-XYZ is defined in Fig. 1(b). The origin is located at the mass center, the Y-axis points upward, the X-axis is parallel to the direction of forwarding motion and the Z-axis complies with the right-hand rule.

Besides, the wing orientation can be obtained in the coordinate frame and with the definition defined in Ref. [8]. In this work, the flapping angle of the right forewing is $80^\circ \pm 3^\circ$, the deviation angle is $68^\circ \pm 3^\circ$, and the pitching angle is $122^\circ \pm 3^\circ$ during the gliding. Besides, the range for each angle during the flapping-gliding flight can also be obtained. It should be noted that, here, the flapping angle, deviation angle, and pitching angle are different from the following because they are obtained from the different coordinates and use different definitions. So here we use ϕ', ψ' and θ' to denote the angles talked about in this part. The orientation of the right hindwing is very close to that of the right forewing. In the present study, for simplicity and due to symmetry, only the right wings are studied. In addition, we choose the position of wings directly measured from the experiments as the baseline case, then carry out

a parametric study to explore the effect of orientation on the aerodynamic performance of the wing in the gliding flight. All the parameters mentioned above are changing within a small range for stability during gliding. For convenience, the averaged measurement values are employed to describe the gliding motion in the paper. The values of related parameters are summarized in Table 1.

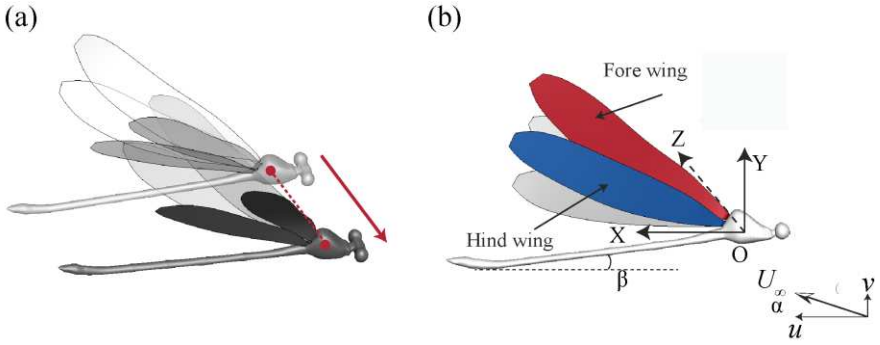

Fig. 1 Snapshot of the damselfly in gliding flight and the definition of the body-fixed coordinates.

Table 1. Summary of the related parameters in gliding flight

β	α	ϕ'		ψ'		θ'	
$8^\circ \pm 2^\circ$	$50^\circ \pm 3^\circ$	$80^\circ \pm 3^\circ$	Range: $-33^\circ \sim 81^\circ$	$68^\circ \pm 3^\circ$	Range: $41^\circ \sim 96^\circ$	$122^\circ \pm 3^\circ$	Range: $92^\circ \sim 136^\circ$

To conveniently change and describe the orientation of wings, a non-inertial wing-root coordinate system (*o-xyz*) is defined in Fig. 2. Here, to make sure that the relative position of forewing and hindwing does not change, we define the midpoint of the forewing root and the hindwing root as the new root of the bi-wing system. Similarly, we define the midpoint of the tips of forewing and hindwing as the tip of the bi-wing system. The origin of the coordinate system is fixed at the new wing root. The y-axis points upward, the root-tip line is along the *x*-axis and the *z*-axis complies with the right-hand rule. The wing orientation is then described using three Euler angles defined in this coordinate: the flapping angle ϕ, the deviation angle ψ, and the pitching angle θ, as shown in Fig. 2(a). It should be noted that, for consistency and convenience, we still use terminologies in the flapping flight to name the orientation angles of a fixed-wing. The flapping angle ϕ is the angular position of the wing in the *xoz* plane around the y-axis. Likewise, the deviation angle ψ is the angular position of the wing with respect to the *z*-axis in the *xoy* plane, as shown in Fig. 2(b). The pitching angle θ defines the angle rotating around the *x*-axis. For the original position of wings, that is, the position directly extracted from the experiments, the flapping angle, deviation angle, and pitching angle are equal to zero in this coordinate system. The definition of the coordinate is similar to that in Ref [9].

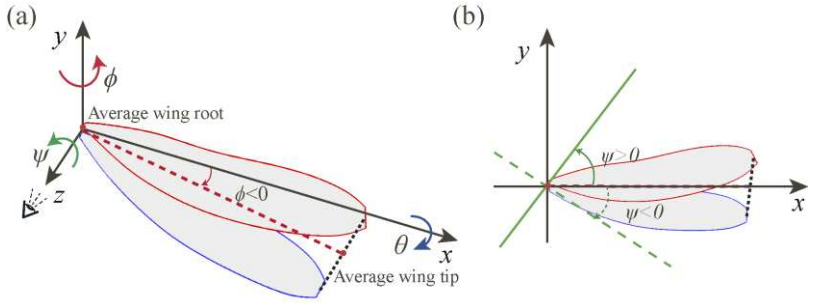

Fig. 2 Schematic of wing orientation in gliding flight

B. Numerical method and simulation setup

In this paper, the equations governing the flow are the three-dimensional unsteady incompressible viscous Navier-Stokes equations, which are written in the non-dimensional form as

$$\frac{\partial u_i}{\partial x_i} = 0, \qquad \frac{\partial u_i}{\partial t} + \frac{\partial u_i u_j}{\partial x_j} = -\frac{\partial p}{\partial x_i} + \frac{1}{Re}\frac{\partial^2 u_i}{\partial x_i \partial x_j} \tag{1}$$

where u_i are the velocity components, p the pressure, and Re the Reynolds number, respectively.

To solve the above equations, a finite-difference-based sharp-interface immersed-boundary method is employed. The equations are discretized on a Cartesian mesh using a second-order central difference scheme and integrated in time using a fractional step method to obtain second-order accuracy. In addition, the boundary conditions are imposed through a ghost-cell procedure. Compared to the body-conformal methods, this method greatly reduces the computational cost for simulations with complex moving boundaries. Besides, when gliding, the forewing and hindwing touch each other, which can introduce difficulties to the simulations, and the level set method has been used in the solver to solve the problem[10]. The method has been widely and successfully applied to simulate biological and bioinspired flow simulations including flying[9, 11-13], swimming[14-17], and biomedical problems[18]. More details and validations about this method can be found in Ref.[10, 19].

In this study, the non-dimensional parameters of Reynolds number are defined as follows,

$$Re = \frac{U_\infty L}{\nu} \tag{2}$$

where U_∞ is the glide speed and $U_\infty = \sqrt{u^2 + v^2}$, L is the root-to-tip length of the forewing, ν denotes the kinematic viscosity. In this study, $Re = 619.8$. Table 2 shows a summary of the important parameters in this extended abstract.

Table 2. Summary of parameters in simulations

U_∞	Re	L	$S_{forewing}$	$S_{hindwing}$
2.48	619.8	1.0	0.298	0.265

The horizontal and vertical forces are normalized separately to quantify the aerodynamic performance of the fixed-wing system,

$$C_X = \frac{F_X}{\frac{1}{2}\rho U_\infty^2 S} \tag{3}$$

$$C_Y = \frac{F_Y}{\frac{1}{2}\rho U_\infty^2 S} \tag{4}$$

where S is the area of a wing. Considering the definition of the body-fixed coordinate and the realistic gliding motion of the damselfly, C_X represents a part of drag of the whole body produced by the wings, and C_Y denotes a part of the lift. For convenience, we call C_X as darg and C_Y as the lift in the following sections. Besides, the ratio of lift to drag is defined as a performance indicator[1],

$$r = \frac{C_Y}{C_X}$$

Usually, a higher ratio r denotes a better gliding flight, because it means that a flyer can move to a further position in the horizontal direction with a certain amount of potential energy.

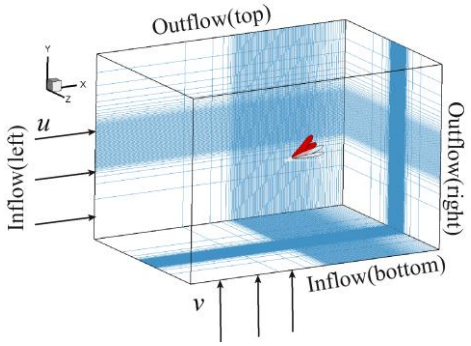

Fig. 3 Schematics of the computational mesh and boundary conditions employed in the present simulations.

As shown in Fig.3, the computational domain has the dimension of $12L \times 8L \times 8L$ in terms of the forewing length to get domain independence results, with $321 \times 225 \times 97$ (approximate 7.0 million) grid nodes in total. A cuboidal dense region with high-resolution grids is designed to solve the flow field near the wings. The minimum grid spacing is set as $\Delta_{min} = 0.013L$. Former convergence studies[20, 21] have proven that the resolution is fine enough at this Reynold number. Considering that we divide the incoming velocity into two directions, the in-flow boundary condition is applied to the left-hand and bottom boundaries, respectively. And the outflow boundary condition is provided at the right-hand and top boundaries. A homogeneous Neumann boundary condition is used for the pressure at all boundaries.

IV. Results and Discussions

In this section, we first present the aerodynamic performance of solitary forewing and hindwing in gliding flight, respectively, and then compare the results with that of the baseline case (the original bi-wing system). Besides, three sets of parametric studies are conducted the explore the effect of the flapping angle, deviation angle, and pitching angle of the damselfly wings on the aerodynamic performance in gliding flight by fixing the other two angles in each set of cases. The horizontal force, vertical force, the force ratio *r* are presented, and three-dimensional vortex structures of different cases are compared and analyzed.

A. Wing-wing interactions in gliding flight of a damselfly

Simulation of solitary wings and the bi-wing system in gliding flight are conducted with the same conditions, and results are compared to study wing-wing interactions in gliding flight of a damselfly. Table 3 summarizes the aerodynamic performance of each case including the single forewing, single hindwing, and forewing and hindwing in the bi-wing system. From the table, it can be seen that compared with the solitary wings, the vertical forces decrease for both wings in the bi-wing system. Meanwhile, in the bi-wing system, C_X of the forewing decreases by 43.9%, while C_X the hindwing increases by 16.7%. Besides, the lift-drag *r* of the forewing in the bi-wing system increases by 14.4%, while that of the hindwing decrease by 17.3%. The vortex structures of each case are shown in Fig. 4.

Table 3. Summary of the aerodynamic performance of solitary wings and the bi-wing system.

		C_Y	C_X	r
forewing(solitary)		0.198	0.132	1.503
hindwing(solitary)		0.258	0.138	1.872
Bi-wing	forewing	0.128	0.074	1.720
	hindwing	0.250	0.161	1.548
Comparison($\frac{\Delta}{solitary\ wing}$%)	forewing	-35.5%	-43.9%	14.4%
	hindwing	-3.1%	16.7%	-17.3%

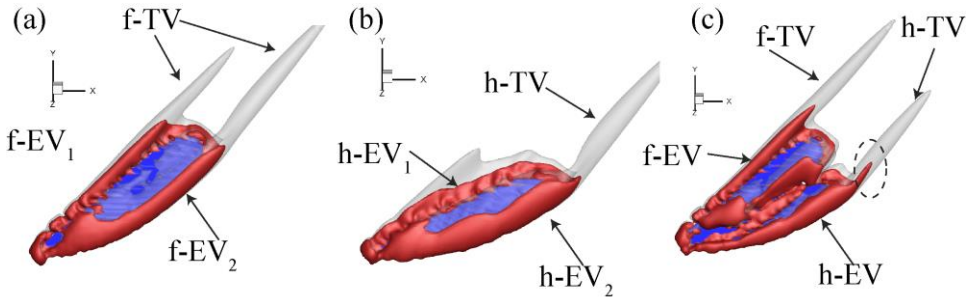

Fig. 4 The vortical structures of (a) solitary forewing, (b) solitary hindwing, and (c) bi-wing system. The vortical structures are visualized by the isosurface of Q-criterion, $Q = 4$ is for the isosurface in gray and $Q = 10$ highlights the vortex core in red.

In Fig. 4, it can be seen that due to the angle between the wing surface and the incoming flow, two edges of a wing both can generate edge vortex(EV) which is the source of lift production. In the bi-wing system, the forewing and hindwing cannot generate coherent EVs, thus the lift produced by each wing decreases. However, for the hindwing, the main source generating lift is the $\mathrm{h}-\mathrm{EV}_2$ and it is barely influenced by the forewing. Therefore, C_Y of the hindwing decreases just by 3.1%. On the other hand, $\mathrm{f}-\mathrm{EV}_2$ is greatly influenced by the hindwing, so C_Y of the forewing decreases a lot. Besides, we can see that one of the tip vortices (TV) of the forewing disappears in the bi-wing system. Thus, the induced drag of the forewing decreases. However, in Fig. 4(c), h-TV gets strengthened, which increases C_X of the hindwing.

It can conclude that in the gliding flight of a damselfly, due to the wing-wing interaction, the lift and drag on the forewing decrease, but its gliding performance is improved. For the hindwing, even though it can maintain lift production, the drag increases a lot, which is detrimental to the gliding performance.

B. Effect of the flapping angle on the aerodynamic performance of damselfly in gliding flight

The lift, drag, lift-drag ratio and three-dimensional vortex structures of the bi-wing system with different flapping angles are studied in this section. From Fig. 5 (a), it can be seen that C_X increases with the increasing flapping angle, no matter for the wings in the system or the system. When $\phi = 0^{\circ}$, C_X of the bi-wing system is comparatively small and is equal to 0.377. In Fig. 4(b), C_Y of the bi-wing system also increases with the increasing flapping angle. When $\phi = 0^{\circ}$, the lift of the bi-wing system is 0.236. In Fig. 5(c), the lift-drag ratio reaches to the maximum, r=1.60, at $\phi = 0^{\circ}$, which means the wings of a damselfly are at the optimum flapping angle in experiments. We define the plane that passes through the damselfly body as the body plane (see Fig. 5(a)). For most birds, when gliding, their wings are unfolded and located at the body plane. However, from the results, it can be concluded that even though when the wings of a damselfly are far away from the body plane, the lift is lower, the lift-drag ratio is higher and the glide performance is improved, which is different from the gliding flight of a bird.

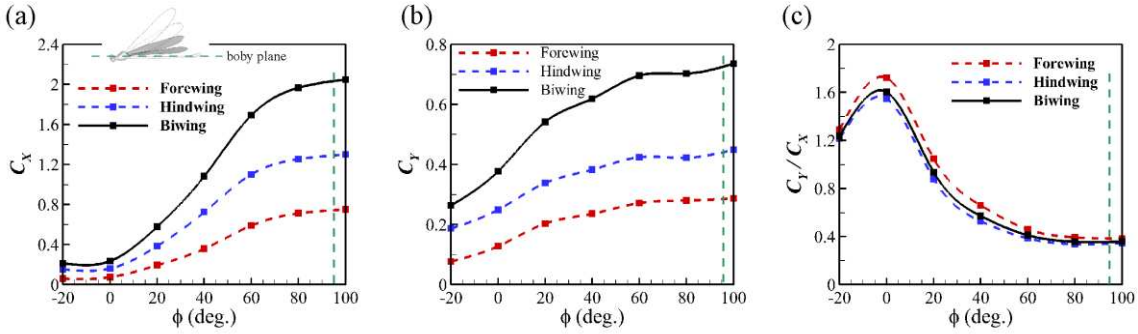

Fig. 5 (a) C_X, (b) C_Y and (c) the lift-drag ratio r of damselfly wings with different flapping angles in gliding flight. The dashed red lines denote the results of the forewing, the dashed blue lines are the results of the hindwing, and the solid black lines are that of the bi-wing system. 0° is the baseline case. The green dashed line denotes the position of the body plane.

Next, we choose three cases including $\phi = -20^{\circ}$, $\phi = 0^{\circ}$ and $\phi = 80^{\circ}$ to make a comparison by presenting vortical structures, surface pressure, and the 2-D vortex slice. In Fig. 6, it can be seen that when $\phi = -20^{\circ}$ at which the wings are almost vertical to the body plane, the vortex structures on the wing surface are weak, which also can be seen from the 2-D vortex slices (see Fig. 6(a2)). Thus, the pressure on the wing surface is slight (see Fig. 6(a3)), and C_X and C_Y of this case are small. On the contrary, when $\phi = 80^{\circ}$, the wing surface is located around the body plane and is vertical to the velocity v, which results in a higher lift. Besides, for this case, the tip vortex is strong, which results in a higher induced drag.

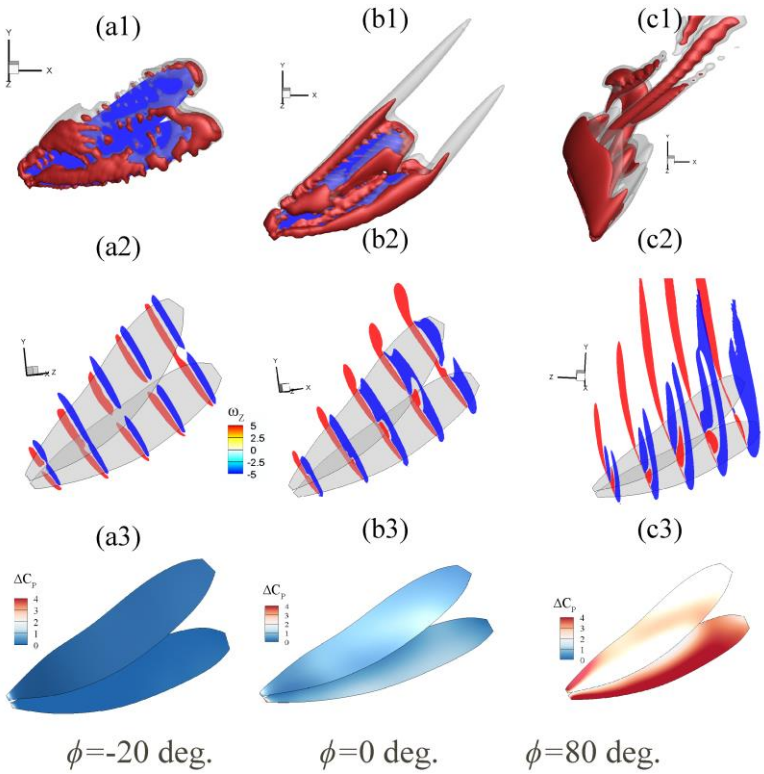

Fig. 6 Comparison of three-dimensional vortex structures (a(1), b(1), c(1)), 2D vortex slices (a(2), b(2), c(2)), and the surface pressure distribution (a(3), b(3), c(3)) of cases with different flapping angles.

C. Effect of the deviation angle on the aerodynamic performance of damselfly in gliding flight

In this section, we fix the flapping angle and pitching angle, but change the deviation angle to study the effect of this angle on the aerodynamic performance of damselfly in gliding flight. The lift, drag, lift-drag ratio of the wings with different deviation angles are presented in Fig. 7. The effect of the deviation angle is investigated by analyzing vortex structures and surface pressure of different cases.

In Fig. 7(a), C_X of the forewing, hindwing and bi-wing system increases with the increasing deviation angle when $\psi < -10^{\circ}$. After that, C_X decreases. When $\psi = -10^{\circ}$, C_X of the bi-wing system reaches the maximum $C_{X\_max} = 0.566$. The variation of C_Y follows a similar trend as C_X when increasing ψ (see Fig. 7(b)). The maximum C_Y of the bi-wing system can be reached at $\psi = -10^{\circ}$ and $C_{Y\_max} = 0.385$. However, the maximum lift-drag ratio r is reached at $\psi = 0^{\circ}$, $r_{max} = 1.602$. Actually, when $\psi = -30^{\circ}$, $r = 1.613 > r_{\psi=0^{\circ}}$. However, $\psi = -30^{\circ}$ is out of the range of deviation angle during the flapping-gliding process presented in Table 1, so it might be difficult for damselfly to keep wings at that angle during gliding. Therefore, the angle is excluded. In conclusion, the best glide performance can be achieved when the wings are at the original position which is extracted from the experiment.

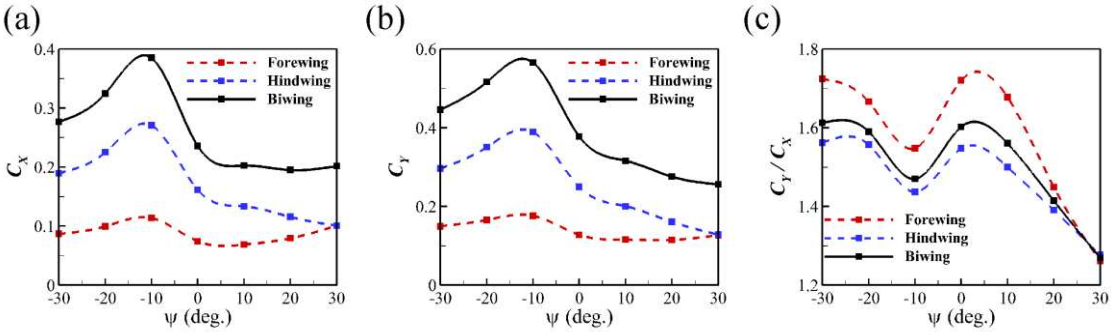

Fig. 7 (a) C_X, (b) C_Y and (c) the lift-drag ratio r of damselfly wings with different deviation angles in gliding flight. The dashed red lines denote the results of the forewing, the dashed blue lines are the results of the hindwing, and the solid black lines are that of the bi-wing system. 0° is the baseline case.

Next, the cases $\psi = -10^\circ$, $\psi = 0^\circ$ and $\psi = 10^\circ$ are chosen to further explore the influence of deviation angle by presenting the 3-D vortex structures, 2-D vortex slices, and surface pressure. In Fig. 8(a1), it can be seen that when $\psi = -10^\circ$, strong and coherent vortex structures are generated at the edges of the bi-wing system, which can also be verified by the 2-D vortex slices in Fig. (a2). Thus, the corresponding surface pressure is higher and a larger lift is produced. On the contrary, when $\psi = 10^\circ$, the vortex structures on the wings are weak and the surface pressure is low. So a lower C_Y is generated. Besides, the tip vortices of the case $\psi = -10^\circ$ is stronger, so the induced drag is larger.

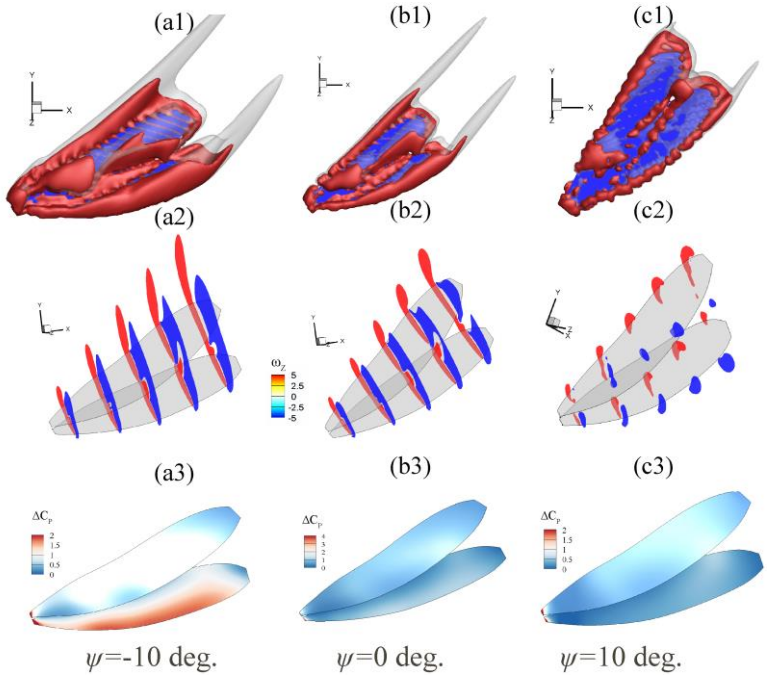

Fig. 8 Comparison of three-dimensional vortex structures (a(1), b(1), c(1)), 2D vortex slices (a(2), b(2), c(2)), and the surface pressure distribution (a(3), b(3), c(3)) of cases with different deviation angles.

D. Effect of the pitching angle on the aerodynamic performance of damselfly in gliding flight

The effect of the pitching angle has been studied by simulating cases with varying the pitching angle and fixing the other two angles. Like the previous parts, the relationships between the aerodynamic performance, including C_X, C_Y and the lift-drag ratio r and the pitching angle are presented. Besides, several cases are selected to be further investigated by comparing their 3-D vortex structures, 2-D vortex slices, and surface pressure.

Fig. 9 shows the variation of C_X, C_Y and the lift-drag ratio r of the damselfly wing when changing the pitching angle in gliding flight. From Fig. 9(a), it can be seen that C_X increases at first, then reaches the maximum value at $\theta = 10^\circ$, finally declines when increasing the pitching angle, no matter for each wing in the system or the bi-wing system. The maximum C_X of the system is 0.259. In Fig. 9(b), C_Y of different wings decrease with the increasing θ, and when $\theta = -10^\circ$, C_{Y_max} of the system is 0.471. From Fig. 9(c), we can see that the ratio r of the system decreases at first, and when $\theta = 20^\circ$, reaches the minimum ($r_{min} = 1.159$), then increases when $\theta > 20^\circ$. The maximum lift-drag ratio of the system is $r_{max} = 2.521$ at $\theta = -10^\circ$. However, similar to the analysis of the deviation angle, by referring to the range of the pitching angle in Table 1, we can notice that it is difficult for a damselfly to keep its wings at $\theta = -10^\circ$ during gliding. We thus can conclude that the original wing orientation can always help the damselfly to improve the gliding performance among the situations with different pitching angles.

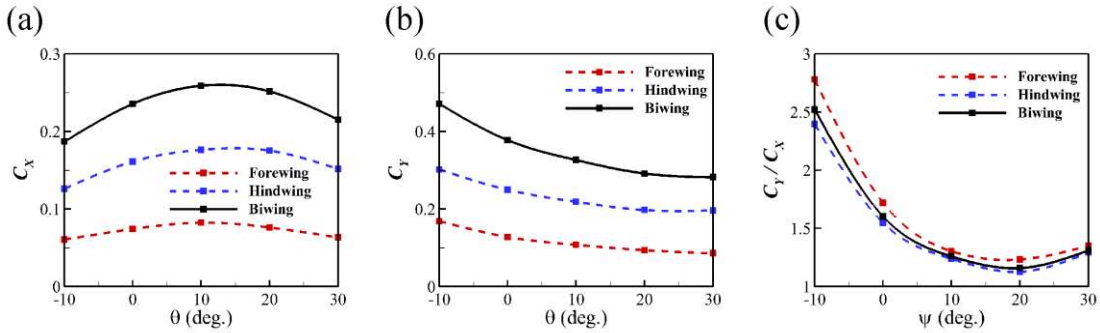

Fig. 9 (a) C_X, (b) C_Y and (c) the lift-drag ratio r of damselfly wings with different pitching angles in gliding flight. The dashed red lines denote the results of the forewing, the dashed blue lines are the results of the hindwing, and the solid black lines are that of the bi-wing system. 0° is the baseline case.

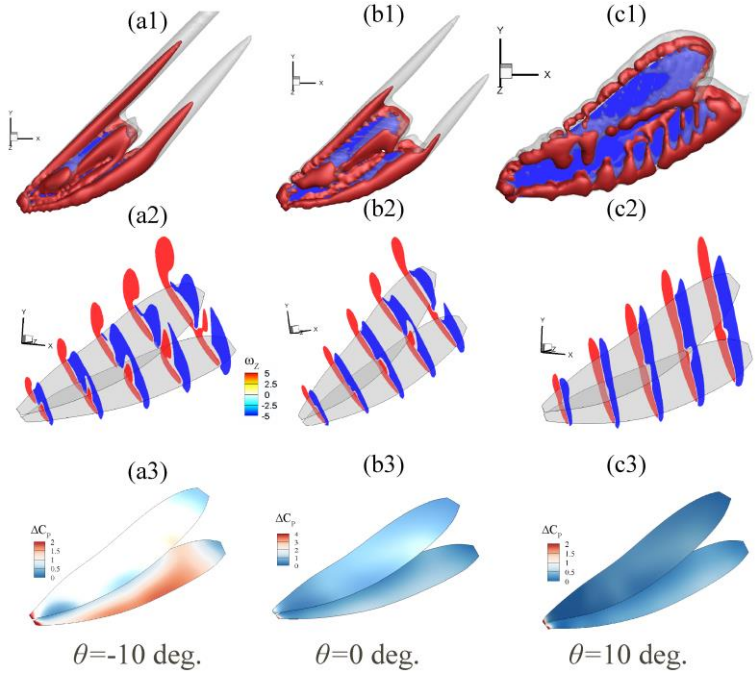

Fig. 10 Comparison of three-dimensional vortex structures (a(1), b(1), c(1)), 2D vortex slices (a(2), b(2), c(2)), and the surface pressure distribution (a(3), b(3), c(3)) of cases with different pitching angles.

Figure 10 presents the vortex structures, 2-D vortex slices, and surface pressure of three cases with different pitching angles including $\theta = -10^{\circ}$, $\theta = 0^{\circ}$, and $\theta = 10^{\circ}$. In Fig. 10(a1) and 10(a3), the strongest edge vortices are generated on the wing surface, and thus a higher lift is produced (see Fig. 9 (b)). Also, the surface pressure for this case is high. On the other hand, when $\theta = 10^{\circ}$, the vortex structures are weak, and thus a smaller lift is generated. Besides, we can find that the tip vortices of the case $\theta = -10^{\circ}$ are stronger, which can help us derive that the induced drag is higher. However, it should also be noticed that the effective angle of attack of this case is shallower, so the pressure drag is smaller. Thus, the resultant drag is small.

V. Conclusion

In this study, a computation study of the gliding flight of a damselfly has been conducted by using an in-house immersed-boundary-method-based numerical solver. The free gliding flight of a damselfly was filmed by using three orthogonally arranged and synchronized high-speed cameras, and the damselfly's wing deformation and kinematics were modeled and reconstructed from the high-speed videos by using a 3D subdivision surface reconstruction methodology. By comparing the aerodynamics of solitary wings and the forewing-hindwing system, it is suggested

that due to the wing-wing interaction, the lift of both forewing and hindwing decreases, and the drag of the forewing also decreases. And the lift-drag ratio of the forewing is improved. Thus, we can conclude that the wing-wing interaction can enhance the gliding performance of the forewing.

Besides, the original wing orientation is measured directly from the experiments and taken as the baseline case in this study. Then, three Euler angles in a wing-root coordinate frame are used to define and vary the wing orientation of the damselfly in gliding flight. The three angles are flapping angle, deviation angle, and pitching angle, respectively. For convenience, we set the three angles of the baseline case as zero in the wing-root coordinate frame. Parametric studies about these three angles have been conducted to investigate the effect of these angles on the aerodynamic performance of the damselfly in gliding flight. It is found that the aerodynamics of the damselfly in gliding is more sensitive to the variation of the flapping angle. And when the wings of the damselfly are at the optimal flapping angle, the wing surfaces are almost vertical to the body plane, which is very different from the observations in bird gliding. It is also found that, for all the three angles, the baseline case, that is, the natural wing orientation of the damselfly in experiments, can achieve the highest gliding performance with $C_X = 0.236$, $C_Y = 0.377$ and $C_Y/C_X = 1.602$. The present study will give insight into the design of micro air vehicles with flapping-gliding flights.

Acknowledgments

This research is supported by NSF CBET-2027534 and NSF CNS-1931929.

References

1. Wakeling, J. M., and Ellington, C. P. "Dragonfly flight. I. Gliding flight and steady-state aerodynamic forces," *Journal of Experimental Biology* Vol. 200, No. 3, 1997, pp. 543-556.
2. Vargas, A., Mittal, R., and Dong, H. "A computational study of the aerodynamic performance of a dragonfly wing section in gliding flight," *Bioinspiration & biomimetics* Vol. 3, No. 2, 2008, pp. 1748-3190.
3. Sanborn, A. F., Villet, M. H., and Phillips, P. K. "Hot-blooded singers: endothermy facilitates crepuscular signaling in African platypleurine cicadas (Hemiptera: Cicadidae: Platypleura spp.)," *Naturwissenschaften* Vol. 90, No. 7, 2003, pp. 305-308.
4. Kovac, M., Vogt, D., Ithier, D., Smith, M., and Wood, R. "Aerodynamic evaluation of four butterfly species for the design of flapping-gliding robotic insects." IEEE, 2012, pp. 1102-1109.
5. Newman, B. G. "Model test on a wing section of a dragonfly," *Scale effects in animal locomotion*, 1977, pp. 445-477.
6. Azuma, A., and Watanabe, T. "Flight performance of a dragonfly," *Journal of Experimental Biology* Vol. 137, No. 1, 1988, pp. 221-252.
7. Li, C., Dong, H., and Zhang, W. "Flying with Abrupt Wing Flapping: Damselfly in Darting Flight," *arXiv preprint arXiv:1310.3325*, 2013.
8. Bode-Oke, A. T., Zeyghami, S., and Dong, H. "Flying in reverse: kinematics and aerodynamics of a dragonfly in backward free flight," *J R Soc Interface* Vol. 15, No. 143, 2018.
9. Pan, Y., Wang, J., and Dong, H. "Study on the passive pitching mechanism of different forms of flapping motion in turning flight," *AIAA Aviation 2019 Forum*. 2019, p. 3435.
10. Pan, Y., Dong, H., and Zhang, W. "An Improved Level-Set-Based Immersed Boundary Reconstruction Method for Computing Bio-Inspired Underwater Propulsion." Vol. 85284, American Society of Mechanical Engineers, 2021, p. V001T02A023.
11. Dong, H., Liang, Z., and Harff, M. "Optimal settings of aerodynamic performance parameters in hovering flight," *International Journal of Micro Air Vehicles* Vol. 1, No. 3, 2009, pp. 173-181.
12. Dong, H., Liang, Z., Wan, H., Koehler, C., and Gaston, Z. "An integrated analysis of a dragonfly in free flight." 2010, p. 4390.
13. Ren, Y., Dong, H., Deng, X., and Tobalske, B. "Video: Turning on a Dime – Asymmetric Vortex Formation in Hummingbird Maneuvering Flight," *68th Annual Meeting of the APS Division of Fluid Dynamics - Gallery of Fluid Motion*. 2015.
14. Han, P., Pan, Y., Liu, G., and Dong, H. "Propulsive performance and vortex wakes of multiple tandem foils pitching in-line," *Journal of Fluids and Structures* Vol. 108, 2022, p. 103422.
15. Pan, Y., and Dong, H. "Computational analysis of hydrodynamic interactions in a high-density fish school," *Physics of Fluids* Vol. 32, No. 12, 2020, p. 121901.

16. Pan, Y., Han, P., Huang, J., and Dong, H. "Effect of Formation Pattern on Schooling Energetics in Fish-Like Swimming," *Fluids Engineering Division Summer Meeting*. Vol. 83730, American Society of Mechanical Engineers, 2020, p. 003T05A046.
17. Narasimhan, M., Dong, H., Mittal, R., and Singh, S. N. "Optimal yaw regulation and trajectory control of biorobotic AUV using mechanical fins based on CFD parametrization," 2006.
18. Zhang, W., Pan, Y., Gong, Y., Dong, H., and Xi, J. "A Versatile IBM-Based AMR Method for Studying Human Snoring." Vol. 85284, American Society of Mechanical Engineers, 2021, p. V001T02A039.
19. Mittal, R., Dong, H., Bozkurttas, M., Najjar, F., Vargas, A., and Von Loebbecke, A. "A versatile sharp interface immersed boundary method for incompressible flows with complex boundaries," *Journal of computational physics* Vol. 227, No. 10, 2008, pp. 4825-4852.
20. Dong, H., Mittal, R., and Najjar, F. M. "Wake topology and hydrodynamic performance of low-aspect-ratio flapping foils," *Journal of Fluid Mechanics* Vol. 566, 2006, pp. 309-343.
21. Zeyghami, S., Zhong, Q., Liu, G., and Dong, H. "Passive pitching of a flapping wing in turning flight," *AIAA Journal* Vol. 57, No. 9, 2019, pp. 3744-3752.